

Mars Science Laboratory Propulsive Maneuver Design and Execution

Mau C. Wong⁽¹⁾, Julie A. Kangas⁽²⁾, Christopher G. Ballard⁽³⁾,
Eric D. Gustafson⁽⁴⁾, and Tomas J. Martin-Mur⁽⁵⁾

⁽¹⁻⁵⁾Jet Propulsion Laboratory, California Institute of Technology
4800 Oak Grove Drive, Pasadena CA 91109 USA
+1-818-354-7405, mau.c.wong@jpl.nasa.gov

Abstract: *The NASA Mars Science Laboratory (MSL) rover, Curiosity, was launched on November 26, 2011 and successfully landed at the Gale Crater on Mars. For the 8-month interplanetary trajectory from Earth to Mars, five nominal and two contingency trajectory correction maneuvers (TCM) were planned. The goal of these TCMs was to accurately deliver the spacecraft to the desired atmospheric entry aimpoint in Martian atmosphere so as to ensure a high probability of successful landing on the Mars surface. The primary mission requirements on maneuver performance were the total mission propellant usage and the entry flight path angle (EFPA) delivery accuracy. They were comfortably met in this mission. In this paper we will describe the spacecraft propulsion system, TCM constraints and requirements, TCM design processes, and their implementation and verification.*

Keywords: *Mars, maneuver, navigation.*

1. Introduction

The NASA Mars Science Laboratory (MSL) rover, Curiosity, was launched on November 26, 2011 and successfully landed at the Gale Crater on Mars on August 6, 2012. The main scientific goal of this rover mission was to determine the habitability of the Martian environment. For that it carried an advanced suite of scientific instruments that included cameras, spectrometers, radiation detectors, and environmental and atmospheric sensors. Further, Curiosity was equipped with the most sophisticated Entry, Descent, and Landing (EDL) system [1] ever assembled for a planetary mission to allow targeting to a desired landing site with unprecedented accuracy. Before it entered the Martian atmosphere, however, Curiosity had to travel 567 million kilometers of interplanetary distance from Earth to Mars. Since there were various constraints and requirements the spacecraft was subjected to during this 8-month journey, a comprehensive navigation system [2] that included orbit determination [3] and maneuver design was needed. Before the Gale Crater was finally selected as the target landing site two months before launch, the MSL mission design and navigation team had been conducting analyses that covered hundreds of possible trajectories. In addition to orbit determination studies, launch vehicle target specification and statistical maneuver studies were done to ensure various flight requirements could be met. Details of the pre-launch trajectory and maneuver analyses will be documented in a separate paper [4]; here we will focus on the post-launch maneuver design and execution.

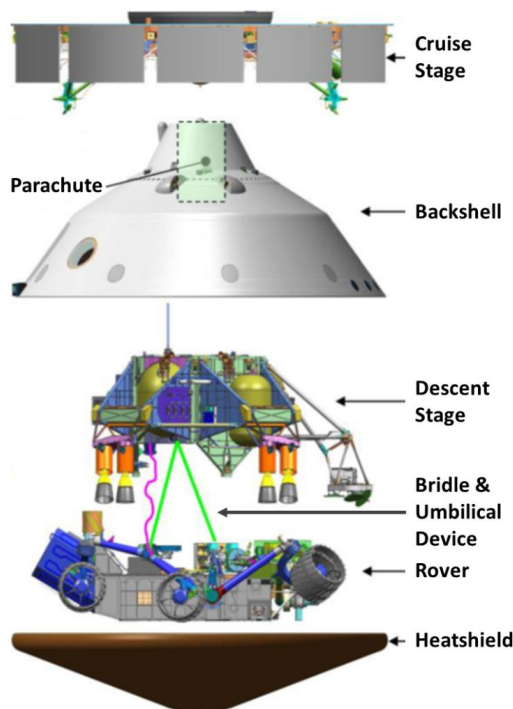
Gale Crater is at about 137.42°E and 4.49°S on Mars surface. Targeting to this landing site was achieved by an atmospheric entry determined by the interplanetary trajectory,

followed by a guided descent through the atmosphere. To ensure a high probability of successful landing, the guided landing profile required an accurate navigation delivery to the atmospheric entry aimpoint, defined at a Mars radius of 3522.2 km (equivalent to 125 km altitude with respect to the Mars equatorial radius.) The atmospheric entry targets were determined iteratively until the spacecraft entry state mapped precisely (an unguided EDL descent profile was used in this process) to the desired landing position. The entry flight path angle (EFPA) was a key parameter that determined the subsequent descent trajectory. Although MSL was equipped with the most advanced EDL system, rigorous trajectory targeting and control were necessary to achieve the atmospheric entry conditions to complement the EDL system for a safe and accurate landing.

The launch injection for the interplanetary trajectory was not directly targeted to the desired entry conditions in the Martian atmosphere, but instead, was targeted to a point that was farther away from the desired aimpoint on Mars b-plane. This was done to satisfy the planetary protection requirements (to be discussed below). Consequently, deterministic TCMs, designed to remove such injection bias, were built into the interplanetary trajectory from Earth to Mars. To account for various knowledge and control errors, including launch vehicle injection errors, orbit determination errors, and maneuver execution errors, additional statistical TCMs were strategically placed. A total of 5 nominal and 2 contingency TCMs were planned.

2. Cruise Stage and Propulsion System

The MSL flight system consisted of four major elements: an interplanetary cruise stage, an aeroshell (composed of a back shell and a heat shield), the descent stage, and the science rover. The flight system components are illustrated in Figure 1. The cruise stage was responsible for transporting the aeroshell to the top of the Martian atmosphere to begin the EDL sequence. The total mass of the flight system at launch was about 3840 kg, of which about 70 kg was the propellant mass allocated for TCM and ACS usages.



2.1 Cruise Propulsion System

The MSL propulsion system was very similar to that of MER. The system was used for spacecraft spin rate correction, altitude control, and all trajectory correction maneuvers. It was a monopropellant hydrazine system, operated in a blow-down mode. There were two spherical propellant tanks each of which contained 36 kg

Figure 1. MSL Flight System Components

of hydrazine at launch. Two clusters (A and B) of four thrusters were diametrically opposed, with each thruster symmetrically canted 40° with respect to the spacecraft's X direction. Each thruster produced about 4.35 N of thrust at the start of the mission, and about 3.09 N for the last maneuver executed. Figures 2 and 3 illustrate the spacecraft axes and thruster configuration. Cluster A contained thrusters 1-4, which have $-X, +Z$ position components. Thrusters 1 and 2 were aligned in the $X-Z$ plane, while thrusters 3 and 4 were aligned parallel to the $X-Y$ plane. Thrusters 5-8 of cluster B were a mirror image of cluster A on the opposite side.

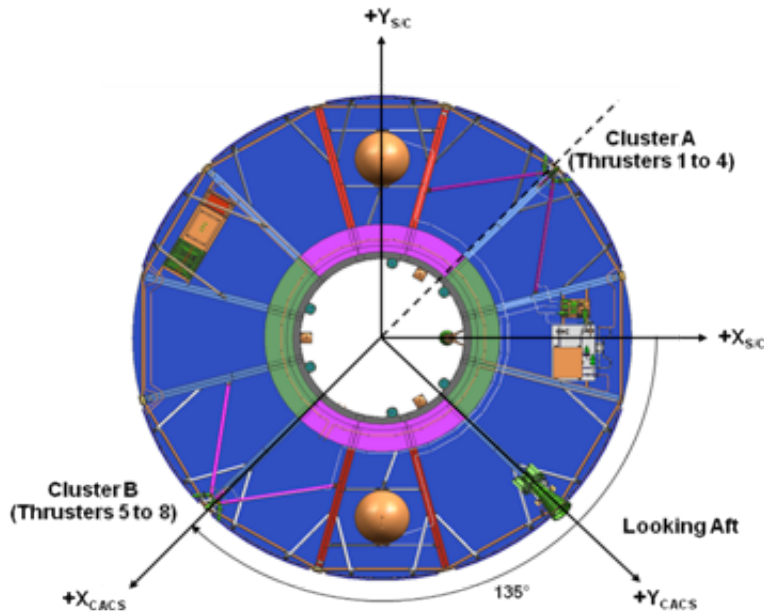


Figure 2. Cruise ACS Frame and Thruster Locations

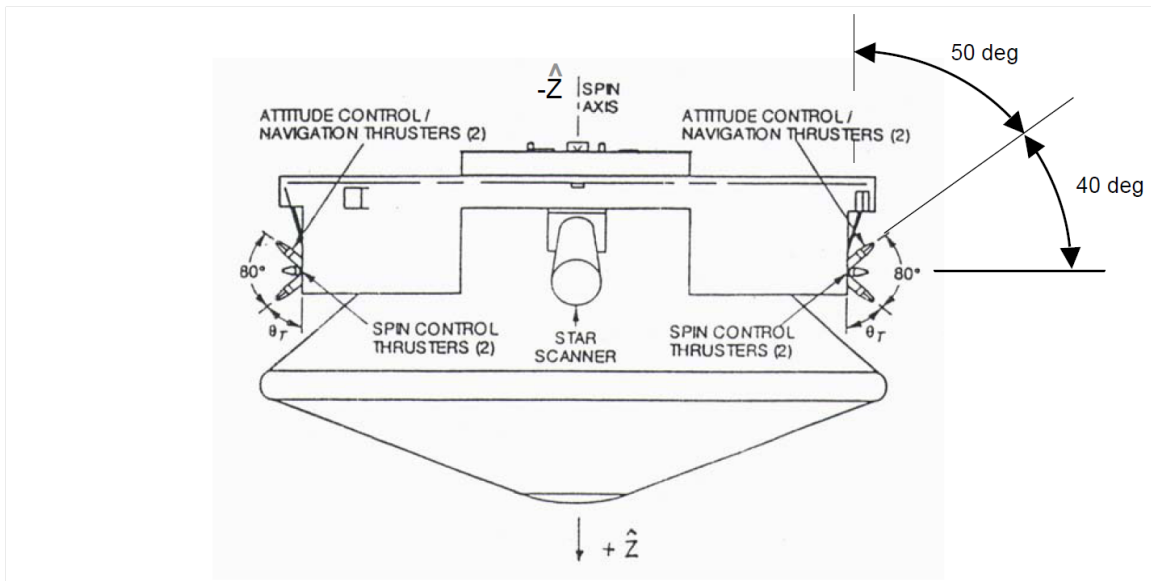


Figure 3. Spacecraft Thruster Configuration

Spacecraft pointing and spin rate control were accomplished by pulse-mode firing of coupled thruster pairs. For example, thruster 3 and 7 were synchronously pulsed to produce a torque in the $-Z$ direction for decrease in angular momentum, or a negative spin rate change. Likewise, thrusters 4 and 8 produced a positive spin rate change. The symmetric thruster alignment produced equal and opposite thrust vectors, resulting in zero net ΔV . Pointing control was achieved in a similar manner. Thrusters 1 and 5 pulsed simultaneously to generate a torque in the spacecraft $-Y$ direction. Half a revolution later, thrusters 2 and 6 pulsed to create a torque in the same inertial direction. The timing of the pulses determined the direction of the precession.

2.2 Propulsive Maneuver Modes

The propulsion design and spin-stabilized system provided a suite of options for implementation of a TCM, but required strict attention to details for accurate propulsive maneuver design. Unlike attitude maneuvers that were performed in closed loop, using the Sun sensor or the IMU to assess changes in attitude, all velocity corrections were commanded with burn duration parameters in an open loop process. Axial burns along the spacecraft spin axis were executed with continuous thruster firing. This type of velocity correction could be performed in the spacecraft $+Z$ (thruster 2 and 5) or $-Z$ (thruster 1 and 6) direction.

Lateral burns produced a velocity correction approximately perpendicular (~ 102 deg) to the spin axis and were performed in a pulse mode operation. The four thrusters of one cluster were fired in unison for typically 5 seconds, producing a 60° burn arc at the nominal spin rate of 2 rpm. The timing of the pulse centered the burn arc about the desired inertial clock angle. This burn pulse was followed by a 10-second wait time, and then the 5-second-pulse-10-second-wait-time was repeated for the other cluster. In this manner, a lateral velocity change operated with a 33% duty cycle.

Lateral velocity corrections were further complicated by the need to direct the thrust vector through the estimated spacecraft center of mass, in order to minimize attitude perturbations. Relative to the thruster clusters, the spacecraft center of mass had a $+Z$ component. Thrusters 1 and 6 produced a thrust vector with a $-Z$ component. By reducing their pulse duration, the net thrust from each cluster moved toward the $+Z$ direction. The pulse duration was shortened such that the burn arc remained centered about the same clock angle as the other three thrusters in the cluster.

The propulsive system was designed to be single fault tolerant. That is, all the propulsion functions could still be performed with a single thruster cluster if necessary, albeit in a degraded fashion. The loss of a thruster cluster obviously would eliminate the benefit of coupled-pair thruster firings, resulting in larger attitude perturbation and execution errors.

In addition to the cant angle and impulsive burn arc implementation loss, plume impingement also reduced the burn efficiency. Accounting for all these effects, lateral

burns were more propellant efficient (roughly by a factor of 1.13), but axial burns could be completed in much shorter times.

Selection of the implementation mode for a TCM execution depended on a number of factors: propellant consumption, execution time, and more importantly, operational constraints. To satisfy both the thermal and telecommunication requirements, the spacecraft's attitude could only be pointed within some allowable regions defined by the spacecraft-Sun-Earth geometry. For TCM-1, the spacecraft $-Z$ axis had to be pointed within 65 degrees from Earth and 50 degrees from the Sun.

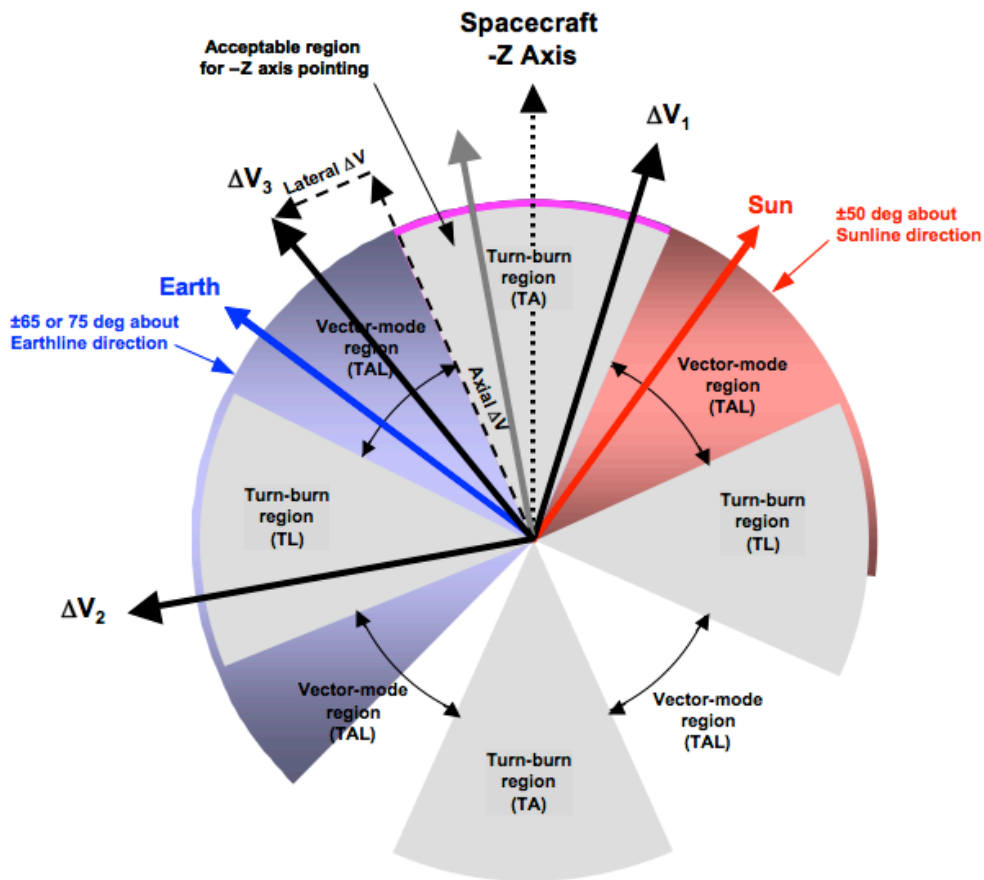


Figure 4. TCM Implementation Schematic

Figure 4 shows a slice through the Sun-spacecraft-Earth plane of the various maneuver implementation zones. The sectors are labeled with the maneuver implementation modes permitted by pointing the spacecraft $-Z$ axis in the allowable region. TA indicates turn and axial burn, TL indicates turn and lateral burn, and TAL indicates turn and vector mode burn. A vector mode (no turn) maneuver implementation is always an option. Also shown are various possible desired ΔV vectors and allowable maneuver implementation modes for these ΔV s. For ΔV_1 , the maneuver is most efficiently accomplished by a turn and axial burn in the $-Z$ direction. For ΔV_2 , the maneuver is most efficiently

accomplished by a turn and lateral burn. For this case, the $-Z$ axis would be pointed as indicated by the gray vector in the allowable $-Z$ axis pointing region. For ΔV_3 , the maneuver can only be accomplished by a turn and vector mode burn. For this case, the $-Z$ axis would be pointed as indicated by the black dashed line labeled “Axial ΔV ” on the borders of the allowable region.

3. TCM Design and Execution

TCM design and execution must achieve the mission requirements while accommodating spacecraft operating constraints. A successful design optimally utilizes the spacecraft capabilities and avoids any unnecessary complexity. A successful execution maintains a level of project reliability and flexibility.

3.1 Interplanetary Trajectory and TCM Location

Five nominal (1-5) and two contingency (5X and 6) TCMs were planned to meet the mission targeting goals and requirements placed on navigation. Table 1 lists the pre-launch planned and post-launch actual TCM locations, relative to launch (L) and entry (E) events. The first three TCMs were placed in the cruise stage of the mission. They were used to shape the interplanetary trajectory such that it was aimed at the nominal atmospheric entry conditions at Mars. The last four (including the two contingency TCMs) were placed in the approach phase of the mission, which began 45 days before entry. The primary purpose of these later TCMs was to fine-tune the trajectory to ensure an accurate atmospheric entry. The orbit determination cutoff (DCO) was seven days before the maneuver execution time for TCM-1, -2, and -3; 13 hours for TCM-4 and -5; and 5 hours for TCM-6. Figure 5 illustrates the TCM locations on the interplanetary trajectory to Mars. The details of the design and execution of each of the TCMs will be discussed below.

Table 1. TCM Schedule

TCM	Pre-launch planned date	Actual execution date	Description
Lateral Calibration	Not planned	Dec. 22, L + 26d	Test of the cruise propulsion system
TCM-1	L + 15d	Jan. 11, L + 46d	Remove injection bias and error, target to the selected landing site.
TCM-2	L + 120d	Mar. 26, L + 121d	
TCM-3	E - 60d	Jun. 26, E - 40d	Correct TCM-2 delivery errors
TCM-4	E - 8d	Jul 28, E - 8d	Correct TCM-3 delivery errors
TCM-5	E - 2d	Waved off	Correct TCM-4 delivery errors
TCM-5X	E - 1d	Not needed	Backup TCM-5 opportunity
TCM-6	E - 9h	Waved off	Contingency opportunity to correct non-survivable delivery errors

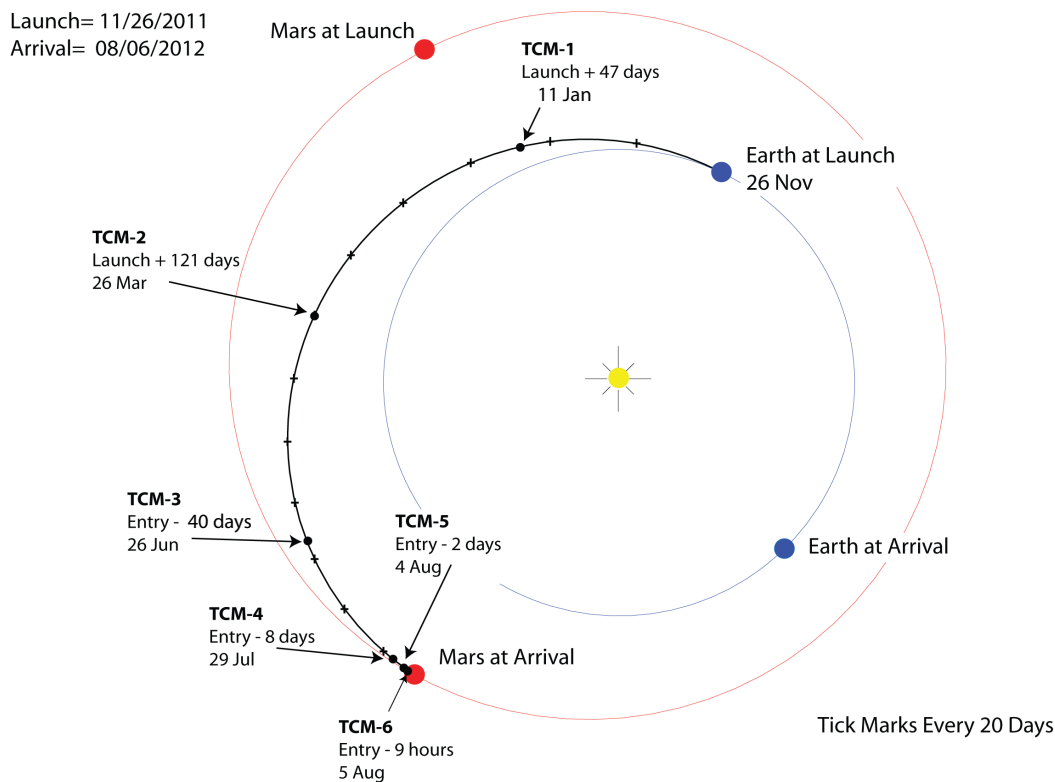


Figure 5. Interplanetary Trajectory and TCM Locations

3.2 Design Constraints and Requirements

MSL navigation had to meet various mission constraints and requirements. A detail account of these constraints and requirements can be found in [2]. Here we will only describe the ones that were relevant to TCM design.

TCM Pointing and Implementation

In terms of operation simplicity, the most straightforward way to implement a TCM is the no-turn vector mode that achieves the desired inertial ΔV by performing an axial/lateral or lateral/axial burn sequence. The no-turn vector mode avoids the unnecessary trajectory perturbations caused by performing turns. It also avoids disruptions to data transmission or event sequencing. However, in anticipation of a possible large TCM-1 ΔV resulting from an off-nominal injection, the prelaunch planned strategy for TCM-1 was to allow the turn-burn mode as an option such that propellant efficiency could be optimized if necessary. The size of the turns would be constrained by the off-Earth and off-Sun angle limitations imposed by thermal and telecommunication systems, as described above. For the same reason, TCM-2 could also be designated as a turn-burn maneuver; however, based on results from pre-launch analyses [4], such arrangement was deemed

unnecessary. Therefore, all subsequent TCMs after TCM-1 were planned as a no-turn vector mode maneuver.

Planetary Protection

- 1) “The probability of Mars impact by the launch vehicle upper stage shall be less than 1.0×10^{-4} ”, and
- 2) “The probability of non-nominal impact of Mars due to failure during the cruise and approach phases shall not exceed 1.0×10^{-2} ”

Requirement 1 had been taken into account when the launch target specification was generated [4]. Requirement 2 was a constraint taken into consideration when TCMs were designed (see Section 3).

TCM Propellant Usage

- 1) “The maneuver design shall ensure a 99% probability of successful targeting to the atmospheric entry point with respect to available propellant”
- 2) “The maneuver design shall ensure that the TCM propellant budget is sufficient with a 90% probability for TCM-1 delayed until launch plus 30 days”

Pre-launch statistical maneuver analyses [4] showed that these requirements were met. Post-launch statistical analyses were also performed along with TCM design during cruise phase to monitor the propellant usage.

Atmospheric Entry Delivery Accuracy

- 1) “The entry vehicle shall be delivered to the specified atmospheric entry conditions with an inertial entry flight path angle error of less than or equal to 0.20 degrees.”

Pre-launch statistical maneuver analyses [4] showed that this requirement was met. Post-launch analysis on delivery accuracy was constantly performed during the approach phase [3]. This requirement also played a role as to determine whether approach-phase TCMs (4-6) were needed.

Maneuver Execution Error

The Gate’s maneuver execution error model was used in all of our statistical analyses, with the following parameters:

	<u>TCM-1</u>	<u>TCMs 2-5</u>
Proportional magnitude error (3σ)	8%	5%
Proportional pointing error, per axis (3σ)	80 mrad	50 mrad
Fixed magnitude error (3σ)	4 mm/s	4 mm/s
Fixed pointing error, per axis (3σ)	4 mm/s	4 mm/s

TCM-1 was assumed to have larger proportional errors because of the lack of prior calibration.

3.3 Design Strategy and Implementation

Since the launch injection was very accurate (with the total error approximately equaled to a $0.23\text{-}\sigma$ value of pre-launch uncertainty estimate), the cruise propellant margin was ample. Consequently, all TCMs were designed as no-turn vector mode maneuvers at their respective cruise attitudes.

3.3.1 Cruise phase TCMs (1-3)

As mentioned above, these TCMs were to use remove injection errors and collectively target the spacecraft to the desired atmospheric entry point in the Martian atmosphere. In order to minimize the propellant usage and satisfy the planetary protection requirements, a chained, multi-maneuver optimization was used. This strategy made use of the different maneuver correction capabilities at different points in the trajectory to come up with an optimal distribution of ΔV 's among the TCMs. The targeted atmospheric entry conditions for the TCMs were the interface radius (r), entry flight path angle (EFPA), and b-plane angle (θ) at an entry time predetermined by the EDL and relay systems. The target radius was fixed at a value of 3522.2 km, which defined the atmospheric entry interface point (AEIP); the EFPA was also fixed at a value of -15.5 degrees, which was required by the EDL system for its optimal performance. Thus, the entry time and b-plane angle are the only two parameters that might vary.

The design algorithm for finding the desired ΔV for a TCM were as follows: The nominal AEIP state and time from the reference trajectory were used as initial states for DSENGS runs (atmospheric descent profile calculations); DSENGS then updated the time and b-plane angle at AEIP required to reach the desired landing site. The processes were iterated until a smooth trajectory from the time of the TCM through landing on the surface.

TCM-1

TCM-1 was designed using a TCM-1/2/3 optimization strategy subjected to the constraints that both TCM-1 and TCM-2 aimpoints in the b-plane had to be some distance away from Mars impact disk. This constraint was imposed to fulfill the non-nominal impact probability requirement. This “safe distance”, based on pre-launch analyses, was 1000 km for TCM-1 and 200 km for TCM-2. Figure 6 shows the TCMs aimpoints in Mars b-plane. Starting from the OD solution, TCM-1 Axial apparently moved the aimpoint farther away from Mars before TCM-1 Lateral brought it back closer to Mars, followed by TCM-2 and -3 which completed the trajectory correction. However, keep in minds that, as shown in the timeline and the colored texts, these aimpoints are being “collapsed” onto a common b-plane. Therefore, the relative spatial distances between these aimpoints are somewhat distorted. Also shown in the figure are the $3\text{-}\sigma$ delivery uncertainties (denoted by colored text and ellipses) associated the OD solution, TCM-1 Axial, and TCM-1 Lateral.

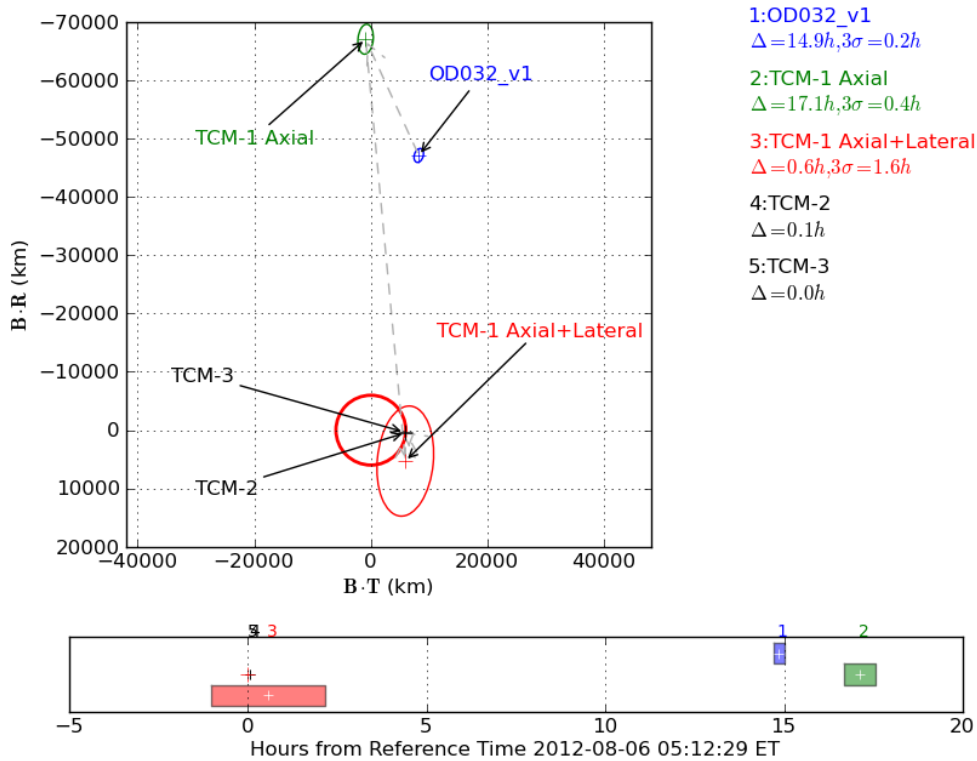


Figure 6. TCM-1, -2, and -3 B-plane Aimpoints

The design yielded three ideal, deterministic ΔV values for each of these three TCMs, which ideally, without any knowledge or control errors, would guide the spacecraft to the desired atmospheric entry conditions in the Martian atmosphere. In actuality, only the TCM-1 design was used; design values for TCM-2 and -3 only served as a reference. The design TCM-1 ΔV was then decomposed into axial and lateral components that together would effect the design ideal ΔV . The decomposition was done in accordance to the propulsion system configuration, as discussed above. Table 2 shows the ideal and implemented ΔV 's, their axial/lateral decompositions, and their contributions in correcting b-plane errors.

The implemented ΔV was the sum of the axial and lateral components. The reason the lateral component alone was greater than the ideal ΔV was that the axial and lateral burn axes were not perpendicular, but at an angle slightly greater 100 degrees. It is seen that TCM-1 was the dominant contributor in correcting the injection errors. The distribution of ΔV 's among the TCMs in a multi-maneuver optimization depends on a number of factors: TCMs location, type of errors to be corrected (temporal/spatial), trajectory characteristics (type 1/2), and target location (latitude/longitude).

Also shown in Table 2 are TCM-1 implementation details including burn duration and propellant usage. Statistical analysis showed that, with such TCM-1, the 99% mission propellant margin was 29.7 kg, which was an ample margin.

Table 2. Summary of TCM-1 Design and Implementation

Ideal and Implemented ΔV at TCM-1 Design						
	Ideal ΔV (m/s)	Total Implemented ΔV (m/s)	No-turn Vector Mode Implementation Components (m/s)			
			Lateral	+Z	-Z	
TCM-1	5.503	7.196	5.611	--	1.585	
TCM-2	0.813	0.916	0.826	--	0.089	
TCM-3	0.040	0.048	0.041	--	0.007	
Change in Mars B-plane						
	Aimpoint			Deltas		
	B•R (km)	B•T (km)	TCA (UTC)	$\Delta B\bullet R$ (km)	$\Delta B\bullet T$ (km)	ΔTCA (hh:mm)
TCM-1	5298.82	5903.47	6 Aug 2012 05:46:33.26	52406	-2313	-14:16
TCM-2	441.56	5930.08	6 Aug 2012 05:15:58.70	-4857	26	-00:30
TCM-3	343.32	5786.17	6 Aug 2012 05:15:08.49	-98	-143	-00:04
Implementation Details						
Segment	Start Time (UTC)	On Time (hh:mm:ss.xx)	ΔV Mag (m/s)	RA (deg)	DEC (deg)	Prop (kg)
Axial	23:00:00.00	00:19:14.12	1.5853	287.00	15.00	4.472
Lateral	23:24:14.72	00:40:28.45	5.6111	167.474	38.808	13.083
Total	--	02:50:10.88*	5.5031	187.693	45.526	17.555

*Total duration including wait times in between burn segments

The actual implementation of TCM-1 was more complex than what was described above. While the axial component was completed by a continuous thrusting along the $-Z$ axis, the lateral component consisted of nine segments of lateral pulses.

TCM-2

While the original plan was to continue the multi-maneuver optimization in the design of TCM-2; that is, the TCM-2 design would also involve TCM-3. It was, however, found that the propellant saving achieved by such optimization was insignificant, given the ample propellant available after TCM-1, and that the non-nominal impact probability requirement could be satisfied without biasing the TCM-2 aimpoint from Mars. Therefore, it was decided to aim TCM-2 directly to the desired atmospheric entry point. A simple, direct ΔV targeting was used. Figure 7 shows TCM-2 aimpoints on b-plane.

Starting from OD solution, TCM-2 Axial and TCM-2 Lateral progressively moved the aimpoint toward the desired final aimpoint.

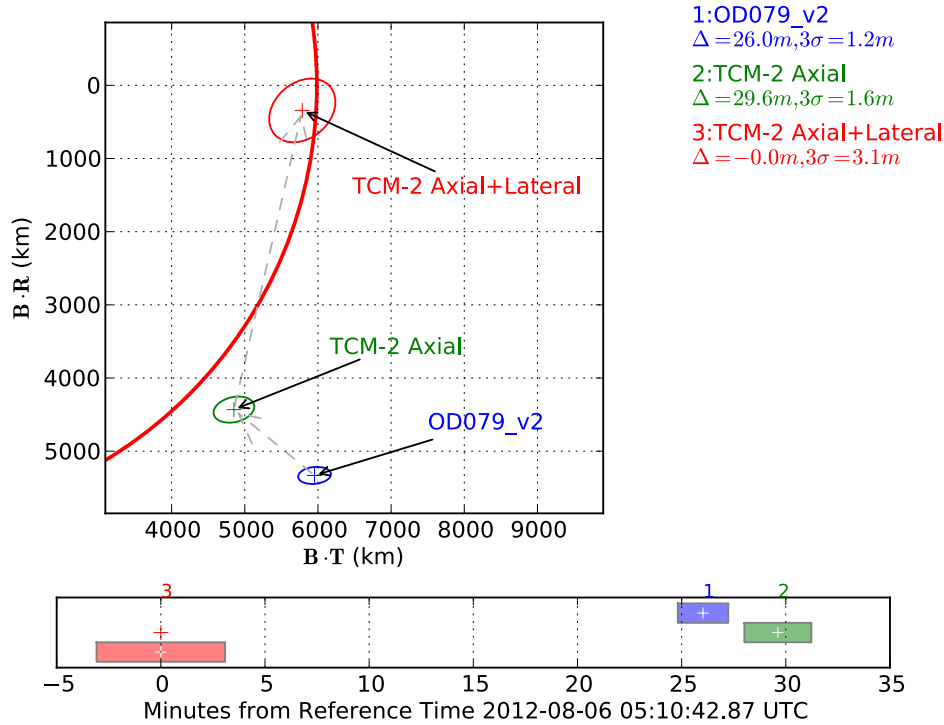


Figure 7. TCM-2 B-plane Aimpoints

Table 3 shows the ideal and implemented ΔV 's, their axial/lateral decompositions, and their contributions in correcting b-plane errors. It is seen that the magnitude of TCM-2 was slightly less than 1 m/s and had roughly the same Axial/Lateral magnitude ratio as that of TCM-1. Also shown are TCM-2 implementation details, including burn duration and propellant usage. Post-launch statistical study showed that the post-TCM-2 99% propellant Margin was 36.29 kg – more than half of the total available propellant. From this point on, propellant margin was no longer a mission's concern.

Table 3. Summary of TCM-2 Design and Implementation

Ideal and Implemented ΔV at TCM-2 Design						
	Ideal ΔV (m/s)	Total Implemented ΔV (m/s)	No-turn Vector Mode Implementation Components (m/s)			
			Lateral	+Z	-Z	
TCM-2	0.712	0.922	0.726	--	0.195	
Change in Mars B-plane						
	Aimpoint			Deltas		
	B•R (km)	B•T (km)	TCA (UTC)	$\Delta B•R$ (km)	$\Delta B•T$ (km)	ΔTCA (hh:mm)
TCM-2	343.07	5786.45	6 Aug 2012 05:10:42.87	-5000.3	-148.4	-00:21
Implementation Details						
Segment	Start Time (UTC)	On Time (hh:mm:ss.xx)	ΔV Mag (m/s)	RA (deg)	DEC (deg)	Prop (kg)
Axial	19:00:00.00	00:02:54.03	0.1954	311.874	-11.731	0.535
Lateral	19:39:53.74	00:05:49.40	0.7265	218.415	67.407	1.684
Total	--	00:57:12.76*	0.7115	253.929	62.484	2.219

*Total duration including wait times in between burn segment

TCM-3

After TCM-2 execution the MSL project decided to shift the target landing point on Mars surface by a few kilometers to land closer to the science target. TCM-3's role was to make adjustment for this small change, in addition to cleaning up the knowledge and control errors accumulated since TCM-2. Again, a simple, direct ΔV targeting strategy was used for the design of TCM-3.

Figure 8 shows TCM-3 aimpoints. Starting from the OD solution, the TCM-3 Axial and Lateral progressively moved towards the desired final aimpoint. It is noted that, after the execution of TCM-2, MSL was on an impact trajectory. *If TCM-3 were not executed*, this would have been a non-nominal impact.

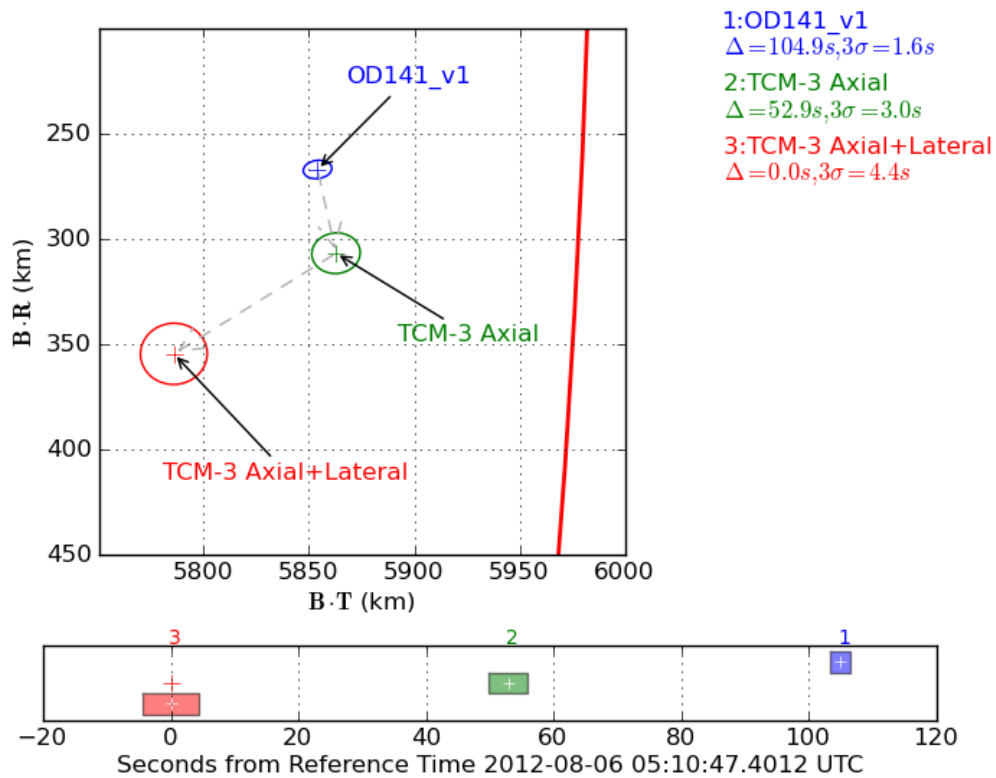


Figure 8. TCM-3 Aimpoints

Table 4. Summary of TCM-3 Design and Implementation

Ideal and Implemented ΔV at TCM-3 Design						
	Ideal ΔV (mm/s)	Total Implemented ΔV (mm/s)	No-turn Vector Mode Implementation Components (mm/s)			
			Lateral	+Z	-Z	
TCM-3	44.359	53.284	25.597	27.687	--	
Change in Mars B-plane						
	Aimpoint			Deltas		
	B•R (km)	B•T (km)	TCA (UTC)	$\Delta B\cdot R$ (km)	$\Delta B\cdot T$ (km)	ΔTCA (mm:ss.xx)
TCM-3	354.77	5785.83	6 Aug 2012 05:10:47.40	-87	68	00:35.80
Implementation Details						
Segment	Start Time (UTC)	On Time (hh:mm:ss.xx)	ΔV Mag (m/s)	RA (deg)	DEC (deg)	Prop (kg)
Axial	17:00:00.00	00:00:27.17	0.0277	174.898	1.030	0.079
Lateral	17:37:27.06	00:00:12.82	0.0256	243.656	-52.933	0.059
Total	--	00:38:04.84*	0.0414	198.279	-28.807	0.138

* Total duration including wait times in between burn segments

3.3.2 Approach Phase TCMs (4, 5, 5X, and 6)

As MSL was getting closer to Mars during the approach phase, the maneuver capability to make changes to the trajectory decreased significantly. The same targeting strategy that applied to earlier TCMs was no longer optimal; in fact, as had been demonstrated by MER navigation analyses [5], the strategy of targeting to three entry conditions in Mars atmosphere was not necessary, nor desirable in some scenarios. As the distance to Mars decreases, the EFPA and entry time become highly correlated. To simultaneously correct for these two parameters could potentially require a large ΔV . Furthermore, a sequence of axial/lateral (or lateral/axial) burns may cause the landing point to exhibit undesirable features; for example, the axial burn may initially move the landing point away from the target before the lateral burn can do the final correction. This situation was indeed encountered in our preliminary TCM-4 design (below). Therefore, we adopted a different targeting strategy that reduced the number of entry parameters being directly targeted to.

The lateral only and axial only strategies targeted the spacecraft to the landing location only and allowed the conditions at AEIP to vary. The spacecraft trajectory without the maneuver was initially propagated to the AEIP and then propagated to the ground using DSENDS. Previously calculated partial derivatives of landing latitude and longitude with respect to the Cartesian components of the TCM were then used to determine an approximate TCM magnitude and direction; the trajectory was then updated with the calculated maneuver. Typically a few iterations were needed for the solution to converge. The axial only maneuver was only able to produce a maneuver along the positive or -Z axis of the spacecraft and so was only able to converge to a minimum distance between the landing site target and the final design. The lateral only maneuver could be in any angle around the spacecraft Z axis and so was able to target the spacecraft directly to the landing site target, at the expense of a small error in entry flight path angle.

TCM-4

Initially all three maneuver options, namely, vector mode, axial only, and lateral only were analyzed for the design of TCM-4. Table 5 shows the OD solution without the maneuver propagated to the ground and the preliminary design options. Figure 9 shows the resulting locations on the ground. The open loop propagation to the ground misses the target by approximately 39 km and is shown in green in the figure. The vector mode maneuver corrected, within iteration tolerances, the miss distance as well as the entry flight path angle. However, because the vector mode maneuver corrects time of flight, flight path angle, and b-plane angle, very often the first component of the maneuver may take the spacecraft away from the target. This is shown in blue, with the label ‘Vector: Axial Component’, in the figure. Only after the lateral component is the spacecraft targeted directly to the landing site target.

The lateral only maneuver corrected the miss distance but does not entirely correct the entry flight path angle to the nominal value, however the difference is negligible and well

within the requirements. The lateral only maneuver was shorter in duration than the vector mode and was more advantageous in that regard. The axial only maneuver only corrected the ground miss distance to 8 km of the target, shown in black with the label 'Axial Only' in the figure, and was longer than both the vector mode and lateral only mode. The decision was made to use the lateral only mode for the final design of TCM-4, which is shown in Table 6.

Table 5. Preliminary TCM-4 Design Options

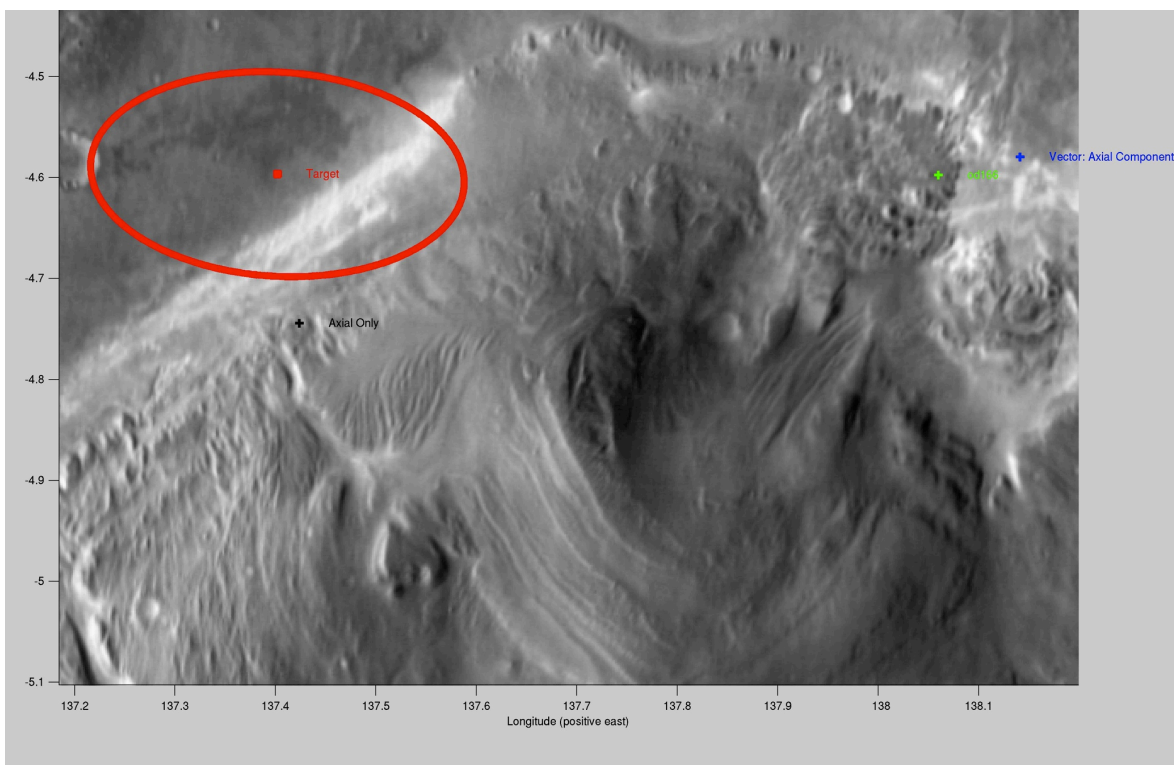
	OD166	TCM-4 Vector	TCM-4 Lateral	TCM-4 Axial
<i>Maneuver</i>				
Axial ΔV (mm/s)		-8.93		72.25
Axial Duration (sec)		8.62		69.69
Lateral ΔV (mm/s)		13.66	10.96	
Lateral Duration (sec)		20.88	16.61	
<i>B-Plane (06-AUG-2012)</i>				
B.R (km)	352.6	355.0	355.1	370.9
B.T (km)	5792.3	5785.2	5785.1	5783.7
B Magnitude (km)	5803.0	5796.1	5796.0	5795.6
TCA (UTC)	05:14:32.87	05:14:33.94	05:14:32.18	05:14:19.27
<i>Entry Conditions (MME of Date at Radius = 3522.2 km, 06-AUG-2012)</i>				
FPA (deg)	-15.2504	-15.4997	-15.5026	-15.5124
B-plane Angle (deg)	3.4798	3.5087	3.5090	3.6660
Epoch (UTC)	05:10:49.71	05:10:47.34	05:10:45.55	05:10:32.50
<i>Landing Conditions (Gale, Open Loop, 06-AUG-2012)</i>				
Landing Time (UTC)	05:17:01.35	05:16:57.04	05:16:55.20	05:16:34.85
Latitude (deg)	-4.597	-4.597	-4.597	-4.744
ΔLatitude (km)	-0.053	-0.004	-0.000	-8.742
E. Longitude (deg)	138.060	137.403	137.402	137.424
ΔE. Longitude (km)	38.854	0.043	0.003	1.298
Total Miss Distance (km)	38.854	0.043	0.003	8.838

Table 6. Final TCM-4 Design Options and Lateral Implementation

	OD169	TCM-4 Lateral
<i>Maneuver</i>		
Axial ΔV (mm/s)		
Axial Duration (sec)		
Lateral ΔV (mm/s)		11.05
Total Lateral Duration (sec)		16.69
<i>B-Plane (06-AUG-2012)</i>		
B.R (km)	352.8	355.1
B.T (km)	5792.4	5785.2
B Magnitude (km)	5803.2	5796.1
TCA (UTC)	05:14:32.91	05:14:32.20
<i>Entry Conditions (MME of Date at Radius = 3522.2 km, 06-AUG-2012)</i>		
FPA (deg)	-15.2447	-15.5027
B-plane Angle (deg)	3.4820	3.5091
Epoch (UTC)	05:10:49.83	05:10:45.56
<i>Landing Conditions (Gale, Open Loop, 06-AUG-2012)</i>		
Landing Time (UTC)	05:17:02.47	05:16:55.21
Latitude (deg)	-4.600	-4.597
Δ Latitude (km)	-0.220	-0.000
E. Longitude (deg)	138.074	137.402
Δ E. Longitude (km)	39.719	0.004
Total Miss Distance (km)	39.720	0.004

Segment	Start Time (UTC)	On-Time (hh:mm:ss.xx)	ΔV Mag. (m/s)	RA (deg)	DEC (deg)	Prop. (kg)
Lateral	05:00:00.00	00:00:05.69	0.0111	268.692	-45.479	0.026
Total	—	00:00:16.71*	0.0111	268.692	-45.479	0.026

Figure 9. TCM-4 Options and Open-Loop Landing Locations



TCM-5

After the successful execution of TCM-4, expectation was that TCM-5 would not be needed. The TCM-5 decision criterion, established earlier based on findings from ORTs, was applied to determine whether or not to perform TCM-5. The criterion took into account the benefit/risk factors of executing TCM-5 and those of performing late EPU on the EDL system. Figure 10 illustrates the criterion in terms of b-plane coordinates. The intersection of the two perpendicular dashed lines denotes the desired final aimpoint. The sets of colored parallel lines represent the EFPA corridors of different widths, with the outermost black lines denoting 0.2 deg from the centerline, yellow 0.1 deg, and green 0.05 deg. The yellow and green pairs are also bounded on top and bottom forming the “Yellow Box” and “Green Box”. Qualitatively, these boxes represent EDL’s capability in correcting EFPA and cross-track errors. Also depicted is the final OD solution for TCM-5 design. The blue ellipse denotes the associated 3- σ OD uncertainties. The criterion was that if the center of the ellipse, i.e., OD best estimate, lay inside the Green Box, no TCM-5 would be needed. Obviously from the figure, this was indeed the case and TCM-4 was the last maneuver executed in the mission.

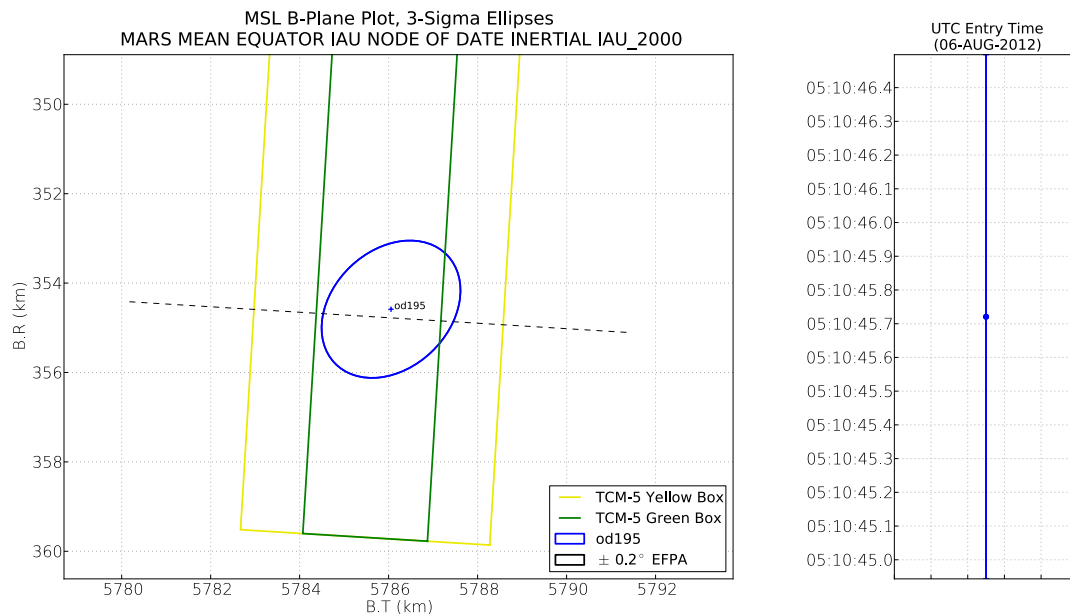


Figure 10. Entry B-plane and EFPA Corridors for TCM-5 Decision

3.4 Verification and Performance

MPF/MIF Verification

For each of the TCMs designed, the navigation and spacecraft teams independently constructed an implementation profile of the ideal ΔV designed by the navigation team. The two profiles, Maneuver Profile File (MPF) from navigation team and Maneuver Implementation File (MIF) from spacecraft team, were then compared to ensure consistency before the final command was sent to the spacecraft for execution.

Tables 7 –10 show the summaries of the comparisons for TCM 1-4, respectively. It is seen that the differences between the two, in terms of the effective ΔV as well as the resulted trajectory correction, were very small. For TCM-4, because of its role in adjusting the final landing location, addition comparison on entry interface parameters and landing location were performed. Again, the differences between the MPF and MIF were negligible.

Table 7. MPF/MIF Comparison for TCM-1

	Parameter	MPF	MIF	Diff (MIF-MPF)
Axial Total	Magnitude (m/s)	1.5853	1.5853	-0.0000
	RA (deg)	287.0000	287.0000	0.0000
	DEC (deg)	15.0000	15.0000	0.0000
	Start Time (UTC)	23:00:00.00	23:00:00.00	00:00:00.00
	On-Time (hh:mm:ss.xx)	00:19:14.72	00:19:14.12	-00:00:00.60
Lateral Total	Magnitude (m/s)	5.6111	5.6111	-0.0000
	RA (deg)	167.5854	167.4739	-0.1114
	DEC (deg)	38.6616	38.8082	0.1466
	Start Time (UTC)	23:24:14.72	23:24:14.72	00:00:00.00
	End Time (UTC)	01:50:34.68	01:50:10.88	-00:00:23.80
	On-time (hh:mm:ss.xx)	–	00:40:28.45	–
Total ΔV	Magnitude (m/s)	5.5031	5.5031	-0.0000
	ΔV_x (m/s)	-3.8313	-3.8206	0.0106
	ΔV_y (m/s)	-0.5225	-0.5161	0.0064
	ΔV_z (m/s)	3.9157	3.9268	0.0112
	B-Plane change	$\Delta \mathbf{B} \cdot \mathbf{R}$ (km)	52476.1	52212.7
$\Delta \mathbf{B} \cdot \mathbf{T}$ (km)		-2299.8	-2168.7	131.1358
ΔTCA (hh:mm:ss.xx)		-14:17:12.16	-14:15:08.26	00:02:03.90

Table 8. MPF/MIF Comparison for TCM-2

	Parameter	MPF	MIF	Diff (MIF-MPF)
Axial Total	Magnitude (m/s)	0.1951	0.1954	0.0003
	RA (deg)	311.8745	311.8740	-0.0005
	DEC (deg)	-11.7313	-11.7310	0.0003
	Start Time (UTC)	19:00:00.00	19:00:00.00	00:00:00.00
	On-Time (hh:mm:ss.xx)	00:02:53.74	00:02:54.03	00:00:00.29
Lateral Total	Magnitude (m/s)	0.7265	0.7265	0.0000
	RA (deg)	218.4651	218.4150	-0.0501
	DEC (deg)	67.2422	67.4070	0.1648
	Start Time (UTC)	19:39:53.74	19:39:53.74	00:00:00.00
	End Time (UTC)	19:57:09.42	19:57:12.76	00:00:03.34
	On-time (hh:mm:ss.xx)	–	00:05:49.40	–
Total ΔV	Magnitude (m/s)	0.7115	0.7115	-0.0000
	ΔV_x (m/s)	-0.0925	-0.0910	0.0015
	ΔV_y (m/s)	-0.3170	-0.3159	0.0012
	ΔV_z (m/s)	0.6303	0.6310	0.0008
B-Plane change	$\Delta \mathbf{B} \cdot \mathbf{R}$ (km)	-4988.1	-5000.3	-12.2693
	$\Delta \mathbf{B} \cdot \mathbf{T}$ (km)	-167.3	-148.4	18.8273
	ΔTCA (hh:mm:ss.xx)	-00:21:39.82	-00:21:29.99	-00:00:09.83

Table 9. MPF/MIF Comparison for TCM-3

	Parameter	MPF	MIF	Diff (MIF-MPF)
Axial Total	Magnitude (m/s)	0.0277	0.0277	-0.0000
	RA (deg)	174.8979	174.8980	0.0001
	DEC (deg)	1.0305	1.0300	-0.0005
	Start Time (UTC)	17:00:00.00	17:00:00.00	00:00:00.00
	On-Time (hh:mm:ss.xx)	00:00:27.06	00:00:27.17	00:00:00.11
Lateral Total	Magnitude (m/s)	0.0256	0.0256	0.0000
	RA (deg)	243.5847	243.6560	0.0713
	DEC (deg)	-53.1160	-52.9330	0.1830
	Start Time (UTC)	17:37:27.06	17:37:27.06	00:00:00.00
	End Time (UTC)	17:38:04.78	17:38:04.84	00:00:00.06
	On-time (hh:mm:ss.xx)	–	00:00:12.82	–
Total ΔV	Magnitude (m/s)	0.0414	0.0414	0.0000
	ΔV_x (m/s)	-0.0344	-0.0344	-0.0000
	ΔV_y (m/s)	-0.0113	-0.0114	-0.0001
	ΔV_z (m/s)	-0.0200	-0.0199	0.0000
B-Plane change	$\Delta \mathbf{B} \cdot \mathbf{R}$ (km)	87.5	87.3	-0.2196
	$\Delta \mathbf{B} \cdot \mathbf{T}$ (km)	-68.2	-68.4	-0.1423
	ΔTCA (hh:mm:ss.xx)	-00:01:09.86	-00:01:09.99	00:00:00.13

Table 10a. MPF/MIF Comparison for TCM-4

	Parameter	MPF	MIF	Diff (MIF-MPF)
Lateral Total	Magnitude (m/s)	0.0111	0.0111	-0.0000
	RA (deg)	268.6894	268.6920	0.0026
	DEC (deg)	-45.6738	-45.4790	0.1948
	Start Time (UTC)	05:00:00.00	05:00:00.00	00:00:00.00
	End Time (UTC)	–	05:00:16.71	–
	On-time (hh:mm:ss.xx)	–	00:00:05.69	–
Total ΔV	Magnitude (m/s)	0.0111	0.0111	-0.0000
	ΔV_x (m/s)	-0.0002	-0.0002	-0.0000
	ΔV_y (m/s)	-0.0077	-0.0077	-0.0000
	ΔV_z (m/s)	-0.0079	-0.0079	0.0000
B-Plane change	$\Delta \mathbf{B} \cdot \mathbf{R}$ (km)	2.3	2.3	-0.0231
	$\Delta \mathbf{B} \cdot \mathbf{T}$ (km)	-7.4	-7.4	-0.0070
	ΔTCA (hh:mm:ss.xx)	-00:00:00.72	-00:00:00.73	00:00:00.01

Table 10b. MPF/MIF Comparison for TCM4 (cont'd)

	OD169	Lateral MPF	Lateral MIF
<i>B-Plane (06-AUG-2012)</i>			
B.R (km)	352.7932	355.0757	355.0527
B.T (km)	5792.4413	5785.1778	5785.1707
B Magnitude (km)	5803.1749	5796.0642	5796.0558
TCA (UTC)	05:14:32.913	05:14:32.204	05:14:32.200
<i>Entry Conditions (MME of Date at Radius = 3522.2 km, 06-AUG-2012)</i>			
FPA (deg)	-15.2447	-15.5027	-15.5030
B-plane Angle (deg)	3.4820	3.5091	3.5089
Epoch (UTC)	05:10:49.830	05:10:45.561	05:10:45.553
<i>Landing Conditions (Gale, Open Loop, 06-AUG-2012)</i>			
Landing Time (UTC)	05:17:02.474	05:16:55.211	05:16:55.153
Latitude (deg)	-4.600	-4.597	-4.596
ΔLatitude (km)	-0.220	-0.000	0.014
E. Longitude (deg)	138.074	137.402	137.401
ΔE. Longitude (km)	39.719	0.004	-0.037
Total Miss Distance (km)	39.720	0.004	0.039

Performance Evaluation

Based on OD reconstruction of the TCMs, it is found that all TCMs performed well with small execution errors, as compared to baseline assumption (Section 2). Table 11 shows summaries of comparison between the planned and executed ΔV for TCM 1- 4, respectively. Note that the lateral burn component of TCM-1 consisted of nine segments of lateral pulses. For TCM-2, -3, and -4, the lateral burn components were small enough that it could be covered in one segment. Details of the TCM reconstruction can be found in [3].

Table 11. OD Reconstruction of TCMs

Segment	Planned ΔV m/s	Estimated ΔV m/s	Estimated EME 2000 Right Ascension deg	Estimated EME2000 Declination deg	Estimated Propellant Usage kg	Magnitude Error %	Pointing Error deg
<i>Minus Z Axial Burn</i>	1.5853	1.6527	286.696	14.979	4.6619	4.249	0.022
Lateral Segment 1	0.7484	0.7631	167.662	39.253	1.7773	1.973	0.527
Lateral Segment 2	0.7304	0.7457	167.478	39.196	1.7366	2.102	0.437
Lateral Segment 3	0.7138	0.7292	167.400	39.177	1.6988	2.159	0.415
Lateral Segment 4	0.6984	0.7138	167.348	39.167	1.6647	2.199	0.408
Lateral Segment 5	0.6842	0.6996	167.283	39.151	1.6307	2.248	0.403
Lateral Segment 6	0.6710	0.6862	167.253	39.148	1.6004	2.273	0.406
Lateral Segment 7	0.6586	0.6738	167.199	39.136	1.5724	2.315	0.410
Lateral Segment 8	0.6470	0.6622	167.173	39.134	1.5441	2.337	0.417
Lateral Segment 9	0.0593	0.0610	166.472	38.846	0.1449	2.790	0.740
<i>Total Lateral</i>	5.6111	5.7346	167.347	39.169	13.3698	2.201	0.410
<i>Total TCM-1</i>	5.5071	5.6350	188.146	45.937	18.0317	2.323	0.618

Segment	Planned ΔV m/s	Estimated ΔV m/s	Estimated EME 2000 Right Ascension deg	Estimated EME2000 Declination deg	Estimated Propellant Usage kg	Magnitude Error %	Pointing Error deg
<i>Minus Z Axial Burn</i>	0.1954	0.1980	311.871	-11.700	0.5421	1.334	0.001
Lateral Segment 1	0.7265	0.7270	218.150	67.778	1.6852	0.069	0.385
<i>Total TCM-2</i>	0.7116	0.7119	254.555	62.747	2.2273	0.038	0.388

Segment	Planned ΔV m/s	Estimated ΔV m/s	Estimated EME 2000 Right Ascension deg	Estimated EME2000 Declination deg	Estimated Propellant Usage kg	Magnitude Error %	Pointing Error deg
<i>Minus Z Axial Burn</i>	0.028	0.029	174.449	2.176	0.079	4.576	1.231
Lateral Segment 1	0.026	0.025	242.983	-52.453	0.059	-2.078	0.630
<i>Total TCM-3</i>	0.041	0.042	196.836	-26.702	0.138	1.029	2.462

Segment	Planned ΔV m/s	Estimated ΔV m/s	Estimated EME 2000 Right Ascension deg	Estimated EME2000 Declination deg	Estimated Propellant Usage kg	Magnitude Error %	Pointing Error deg
Lateral Segment 1	0.0111	0.0104	266.504	-44.659	0.026	-5.702	1.750
<i>Total TCM-4</i>	0.0111	0.0104	266.504	-44.659	0.026	-5.702	1.750

4. Conclusion

The MSL navigation performance was in general very good and fulfilled all requirements with comfortable margins. This in part contributed to the success of EDL and other MSL subsystems. The OD and maneuver teams together have provided trajectory prediction and control that were far above the mission requirements imposed. In particular, the maneuver team has successfully performed all the trajectory control tasks including the design and implementation of TCMs that in part led to the accurate delivery of the spacecraft to the desired atmospheric entry conditions at Mars. The actual EFPA delivered has been estimated to be only 0.013 degrees off the target values of -15.5

degrees. The adopted maneuver strategy has successfully addressed and fulfilled the constraints imposed by planetary protection and attitude control. Aided by a good injection performance from the launch vehicle, the total TCM/ACS propellant usage was less than half of the allocated 70 kg.

Acknowledgments

The maneuver team would like to thank the excellent support provided by their fellow MSL navigation team members and the ACS team. This research was carried out at the Jet Propulsion Laboratory, California Institute of Technology, under a contract with NASA.

References

- [1] Burkhart, P.D.; Casoliva, J. “MSL DSENGS EDL Analysis and Operations”, 23rd International Symposium on Space Flight Dynamics, Pasadena, CA, USA, 2012.
- [2] Martin-Mur, T.J.; Kruizinga, G.L.; Wong, M.C.; Abilleira, F. “Mars Science Laboratory Navigation Results”, 23rd International Symposium on Space Flight Dynamics, Pasadena, CA, USA, 2012.
- [3] Kruizinga, G.L.; Gustafson, E.D.; Jefferson, D.C.; Martin-Mur, T.J.; Mottinger, N.A.; Ryne, M.S.; Thompson, P.F. “Mars Science Laboratory Orbit Determination Results”, 23rd International Symposium on Space Flight Dynamics, Pasadena, CA, USA, 2012.
- [4] Wong, M.C.; Kangas, J.A. “Mars Science Laboratory Trajectory and Maneuver Analyses”, submitted to 23rd AAS/AIAA Spaceflight Mechanics Meeting, Kauai, Hawaii, USA, 2013.
- [5] Potts, C.L.; Raofi, B.; Kangas, J.A. “Mars Exploration Rovers Propulsive Maneuver Design”, AIAA/AAS Astrodynamics Specialist Conference, AIAA-2004-4985, AIAA, Washington, DC, USA, 2004.